**Climate
of the Past**
Open Access
Discussions

The East Asian winter monsoon variability in response to precession and inter-hemispheric heat balance

M. Yamamoto[1,2], H. Sai[2,*], M.-T. Chen[3], and M. Zhao[4]

[1]Faculty of Environmental Earth Science, Hokkaido University, Kita-10, Nishi-5, Kita-ku, Sapporo, 060-0810, Japan
[2]Graduate School of Environmental Science, Hokkaido University, Kita-10, Nishi-5, Kita-ku, Sapporo, 060-0810, Japan
[3]Institute of Applied Geosciences, National Taiwan Ocean University, Keelung, 20224, Taiwan
[4]Key Laboratory of Marine Chemistry Theory and Technology of the Ministry of Education, Ocean University of China, Qingdao, 266003, China
[*]Present address: Hitachi Advanced Systems Corporation, Yokohama, 244-0817, Japan

Correspondence to: M. Yamamoto (myama@ees.hokudai.ac.jp)

CPD

9, 4229–4261, 2013

The East Asian winter monsoon variability

M. Yamamoto et al.

Title Page

Abstract | Introduction

Conclusions | References

Tables | Figures

|◄ | ►|

◄ | ►

Back | Close

Full Screen / Esc

Printer-friendly Version

Interactive Discussion

Abstract

The response of Asian monsoon variability to orbital forcing is still unclear, and all hypotheses are controversial. We present a record of the sea surface temperature difference (ΔSST) between the South China Sea and the other Western Pacific Warm Pool regions as a proxy for the intensity of the Asian winter monsoon, because the winter cooling of the South China Sea is caused by the cooling of surface water at the northern margin and the southward advection of cooled water due to winter monsoon winds. The ΔSST showed significant precession cycles during the last 150 kyr. In the precession cycle, the maximum winter monsoon intensity shown by the ΔSST corresponded to the May perihelion and was delayed behind the maximum ice volume. The East Asian winter monsoon was anti-phase with the Indian summer monsoon and the summer monsoon precipitation in central Japan. The timing of the maximum phase of the East Asian winter monsoon was different from previous results in terms of the March perihelion (ice volume maxima) and June perihelion (minimum of Northern Hemisphere winter insolation). We infer that the variation of the East Asian winter monsoon was caused by a physical mechanism of inter-hemispheric heat balance. The East Asian winter monsoon was intensified by the Northern Hemisphere cooling, which was caused by the combined effect of cooling by the ice volume forcing and the decrease in winter insolation, or by decreased heat transfer from the Southern Hemisphere to the Northern Hemisphere owing to the weak Indian summer monsoon at the May perihelion.

1 Introduction

The Asian monsoon is the largest monsoon system on the Earth and is characterized by inter-hemispheric phenomena (e.g. Wang et al., 2003). It consists of the East Asian and Indian monsoons and is linked with the Australian and African monsoons. While the Indian summer monsoon is stronger than the East Asian summer monsoon, the

East Asian winter monsoon is much stronger than the Indian winter monsoon. In boreal winter, the winter monsoon occurs over East Asia and the adjacent marginal seas and is directly linked to the Australian summer monsoon through cross-equatorial flows over the South China Sea (SCS) (Wang et al., 2003).

Long-term changes in the Asian monsoon are an important topic of paleoclimatology. The Asian monsoon responds to insolation changes at low latitudes, which is regulated by precession, and hence it has been assumed to respond to precessional forcing (Kutzbach, 1981). However, the phase of the monsoon variability is not clear, and the hypotheses are controversial. According to the hypothesis of Kutsbach (1981), the summer monsoon is maximized when the Northern Hemisphere summer insolation is maximal. Chinese loess records have suggested that the East Asian winter monsoon was stronger in glacials than in interglacials (Ding et al., 1995; Xiao et al., 1995). Chinese speleothem records have suggested that the variation in the East Asian summer monsoon was maximal at the July to August perihelion, and the phase is consistent with that of the Kutsbach model (Wang et al., 2001, 2008; Yuan et al., 2004). In contrast, based on marine records, Huang et al. (1997a,b) stressed that monsoon intensity is regulated by glacial conditions. In glacials, the summer monsoon was weaker, and the winter monsoon was stronger. Clemens and Prell (2003) argued that the Indian summer monsoon was the strongest at the November perihelion. These hypotheses assumed different phases of monsoon variation on a precessional cycle.

The South China Sea is a part of the Western Pacific Warm Pool (WPWP) region, but the winter sea surface temperature in the SCS is significantly lower than that in other regions of the WPWP. A recent oceanographic study demonstrated that this winter cooling is caused by the winter monsoon: winter monsoon northerly winds cool the surface water in the northern margin and advect the cooled water southward (Liu et al., 2004). Using this relationship, winter monsoon variations can be reconstructed by generating sea surface temperature (SST) records for the SCS. Shintani et al. (2008) discussed winter monsoon variation over the last 23 000 yr. The temperature difference between the northern SCS and the Sulu Sea suggests that the winter monsoon was

The East Asian winter monsoon variability

M. Yamamoto et al.

Full Screen / Esc

Printer-friendly Version

Interactive Discussion

stronger in the last deglaciation, in particular, during the Younger Dryas period, and that the intensity in the last glacial maximum (LGM) was the same as that in the middle Holocene. Tian et al. (2010) compared Mg/Ca-derived SSTs between the northern and southern SCS and showed that the SST gradient was higher in Heinrich 1 and Younger
5 Dryas periods. Huang et al. (2011) reported that the SST gradient at the western and eastern margins of the southern SCS was higher in Heinrich 2, Heinrich 1 and Younger Dryas periods, suggesting enhanced East Asian winter monsoon activity in these periods. This strategy is useful for understanding the Asian winter monsoon variation, but a longer record is necessary to understand the response of the Asian winter monsoon
10 to orbital forcing.

Many paleoceanographic studies of SST have been conducted in the SCS. Wang and Wang (1990) and Wang et al. (1995) reconstructed summer and winter SSTs in the SCS based on foraminifer assemblages, and found that during the LGM, the SCS experienced larger seasonal SST differences and a steeper latitudinal SST gradient
15 than it does presently. Intense glacial cooling in the northern SCS was reported based on foraminifer- and alkenone-based SST records (Huang et al., 1997a,b; Chen and Huang, 1998; Pelejero et al., 1999; Chen et al., 2003). Kienast et al. (2001) found a millennium-scale temperature variation that mimics Greenland ice core records. Oppo and Sun (2005) and Zhao et al. (2006) reported millennium-scale temperature varia-
20 tions in the northern and southern SCS, respectively, for the last two glacial–interglacial cycles. The glacial–interglacial contrast of SST in the SCS have been attributed to either the inflow of cold water from the North Pacific (e.g. Wang and Wang, 1990; Wang et al., 1995) or changes in the winter monsoon intensity (e.g. Huang et al., 1997a,b). Disagreement regarding estimated paleotemperatures in the SCS was reported among
25 different proxies such as alkenone $U^{K'}_{37}$, the foraminiferal Mg/Ca ratio, and the transfer function. This is potentially attributable to differences in the season and depth that each proxy reflects (e.g. Steinke et al., 2008). Alternative approaches such as TEX_{86} are useful for better understanding paleotemperature change mechanisms in the SCS (Shintani et al., 2011).

TEX$_{86}$ is a recently developed paleotemperature proxy (Schouten et al., 2002) based on glycerol dialkyl glycerol tetraethers (GDGTs). The TEX$_{86}$ paleothermometer has the advantage that it does not appear to be influenced by salinity (Wuchter et al., 2004), and it is more sensitive to temperature changes in tropical waters (Kim et al., 2010) compared with the U$_{37}^{K'}$ method (Pelejero and Grimalt, 1997). TEX$_{86}$ has been applied to paleotemperature estimations in the northern SCS (Shintani et al., 2011; Li et al., 2013). Shintani et al. (2011) assumed that TEX$_{86}$ reflected the SST weighted in warmer seasons, but Li et al. (2013) subsequently assumed that TEX$_{86}$ reflects subsurface temperature, based on the results of a surface sediment study (Jia et al., 2012). In the shallow water region of the SCS, Zhang et al. (2013) suggested that TEX$_{86}$ records a cooler season temperature.

Here, we present records of TEX$_{86}^{H}$-derived temperatures from southern SCS core MD97-2151, which is located offshore from Vietnam, for the last 150 000 yr. We obtained a record of SST differences between the SCS and the central WPWP to understand the Asian winter monsoon variability and mechanisms during the last 150 000 yr.

2 Oceanographic settings

The SCS is a marginal sea of the North Pacific with seven connections through the Taiwan Strait to the East China Sea (sill depth $\sim$ 70 m), the Bashi Strait to the North Pacific (sill depth $\sim$ 2500 m), the Mindoro and Balabac Straits to the Sulu Sea (sill depths $\sim$ 450 and $\sim$ 100 m, respectively), the Malacca Strait to the Indian Ocean (sill depth $\sim$ 30 m), and the Gaspar and Karimata Straits ($\sim$ 40–50 m) to the Java Sea (Fig. 1; Wyrtki, 1961). The surface circulation in the SCS is driven by large-scale, seasonally reversed monsoon winds (Wyrtki, 1961). In the boreal summer, southwesterly winds drive an inflow of Indian Ocean water through the Sunda Shelf and a clockwise surface circulation in the SCS. In the boreal winter, northeasterly winds drive an inflow of North Pacific water through the Bashi Strait, an inflow of East China Sea water through the Taiwan Strait, and a counterclockwise surface circulation in the SCS. The southern SCS is part of the

WPWP region, but the winter surface temperature is significantly lower than that in the central WPWP. A recent oceanographic study demonstrated that this winter cooling is caused by the winter monsoon. Winter monsoon northerly winds cool the surface water in the northern margin of the SCS and advect the cooled water southward (Liu et al., 2004). The SST in the study region is governed by the winter wind strength (Huang et al., 2011). The present-day SST at the study site shows a seasonal variation between 26.0 °C in January and 29.5 °C in May, with a mean annual value of 27.9 °C (Fig. 2; NOAA, 1998).

3 Materials and methods

3.1 Samples and age-depth model

During the IMAGES 1997 Marion Dufresne cruise, a giant piston core (MD97-2151; 26.72 m long) was collected from a water depth of 1598 m on the southwestern slope of the SCS at 8°43.73′ N, 109°52.17′ E (Fig. 1). The sediment that was retrieved consisted of olive to dark gray silty clay with nannofossils, foraminifera, and diatoms (Chen et al., 1998).

The study core was previously investigated based on the oxygen isotopes of planktonic foraminifera (Lee et al., 1999), paleomagnetic properties (Lee, 1999), carbonate content (Huang et al., 1999), foraminiferal assemblage (Huang et al., 2002), and alkenone $U^{K'}_{37}$ and the oxygen isotopes of benthic foraminifera (Zhao et al., 2006).

An age model in calendar years (Fig. 3; Table 1) was created by oxygen isotope stratigraphy (Martinson et al., 1987) of benthic foraminifera *Cibicidoides wuellerstorfi* (Zhao et al., 2006), by one ash layer (Toba ash, 71 ka; Zielinski et al., 1996), and by the AMS ^{14}C ages of 13 samples of the planktonic foraminiferan *Globigerinoides sacculifer*. The ^{14}C age at 699.5 m was not used for the age-depth model. The calendar age was converted from the AMS ^{14}C age using the CALIB5.0 program and marine04.14C dataset (Reimer et al., 2004) with a 400 yr global reservoir correction.

The East Asian winter monsoon variability

M. Yamamoto et al.

A total of 178 samples were collected every 15 cm on average (equivalent to approximately 840-year intervals) down to a depth of 26.7 m (150 ka).

3.2 Lipid extraction and separation

Lipids were extracted (x 3) from 1 g of dried sediment using a DIONEX Accelerated Solvent Extractor ASE-200 at 100 °C and 1000 psi for 10 min with 11 mL of CH_2Cl_2-CH_3OH (6 : 4) and then concentrated. The lipid extract was separated into three fractions using column chromatography (SiO_2 with 5 % distilled water; i.d., 5.5 mm; length, 45 mm): F1-2 (hydrocarbons), 3 mL hexane-toluene (3 : 1); F3 (ketones), 4 mL toluene; F4 (polar compounds), 3 mL toluene-CH_3OH (3 : 1).

3.3 Alkenone analysis

Gas chromatography (GC) of F3 (alkenones) was conducted using a Hewlett Packard 5890 series II gas chromatograph with on-column injection and electronic pressure control systems, and a flame ionization detector. Samples were dissolved in hexane. He was the carrier gas at 30 cm/s. A Chrompack CP-Sil5CB column was used (60 m × 0.25 mm i.d.; film thickness, 0.25 µm). The oven temperature was programmed to rise from 70 to 290 °C at 20 °C min^{-1}, from 290 to 310 °C (held 30 min) at 0.5 °C min^{-1}.

The alkenone unsaturation index $U_{37}^{K'}$ was calculated from the concentrations of di- and tri-unsaturated C_{37} alken-2-ones ([$C_{37:2}$MK] and [$C_{37:3}$MK], respectively) using the following expression (Prahl et al., 1988):

$$U_{37}^{K'} = [C_{37:2}MK] / ([C_{37:2}MK] + [C_{37:3}MK]).$$

Temperature was calculated according to the equation

$$U_{37}^{K'} = 0.031 T + 0.092$$

Full Screen / Esc

Printer-friendly Version

Interactive Discussion

where T is temperature [°C] based on core-top calibration in the SSC (Pelejero and Grimalt, 1997); analytical accuracy (standard deviation in a replicate analysis) was 0.24 °C in our laboratory.

3.4 Glycerol dialkyl glycerol tetraether (GDGT) analysis

Glycerol dialkyl glycerol tetraethers (GDGTs) were analyzed following Yamamoto and Polyak (2009). An aliquot of F4 was dissolved in hexane-2-propanol (99 : 1) and filtered. Glycerol dialkyl glycerol tetraethers (GDGTs) were analyzed using high performance liquid chromatography-mass spectrometry (HPLC-MS) with an Agilent 1100 HPLC system connected to a Bruker Daltonics micrOTOF-HS time-of-flight mass spectrometer. Separation was conducted using a Prevail Cyano column (2.1 × 150 mm, 3 µm; Alltech) and maintained at 30 °C following the method of Hopmans et al. (2000) and Schouten et al. (2007). Conditions were: flow rate 0.2 mL min^{-1}, isocratic with 99 % hexane and 1 % 2-propanol for the first 5 min followed by a linear gradient to 1.8 % 2-propanol over 45 min. Detection was achieved using atmospheric pressure, positive ion chemical ionization-mass spectrometry (APCI-MS). The spectrometer was run in full scan mode (m/z 500–1500). Compounds were identified by comparing mass spectra and retention times with those of GDGT standards (formed from the main phospholipids of Thermoplasma acidophilum via acid hydrolysis) and those in the literature (Hopmans et al., 2000). Quantification was achieved by integrating the summed peak areas in the $(M + H)^+$ and the isotopic $(M + H + 1)^+$ ion traces.

TEX_{86}^H was calculated from the concentrations of GDGT-1, GDGT-2, GDGT-3 and a regioisomer of crenarchaeol using the following expression (Schouten et al., 2002; Kim et al., 2010):

$$TEX_{86}^H = \log TEX_{86} = \log([GDGT\text{-}2] + [GDGT\text{-}3] + [Crenarchaeol\ regioisomer])/$$

$$([GDGT\text{-}1] + [GDGT\text{-}2] + [GDGT\text{-}3] + [Crenarchaeol\ regioisomer]).$$

TEX_{86}^H is defined as the logarithmic function of TEX_{86} and yields the best correlation with SST when the data from polar and subpolar oceans are removed (Kim et al.,

2010). SST was calculated according to the following equation based on a global core-top calibration (Kim et al., 2010):

$$\text{SST} = 68.4 \times \text{TEX}_{86}^{H} + 38.6$$

where SST = sea surface temperature [°C]; analytical accuracy was 0.45 °C in our laboratory.

The temperature at 30–125 m was calculated according to the following equation based on a local core-top calibration in the SCS (Jia et al., 2012):

$$T_{30-125m} = 54.5 \times \text{TEX}_{86}^{H} + 30.7$$

where $T_{30-125m}$ = temperature at 30–125 m [°C]; analytical accuracy was 0.36 °C in our laboratory.

Branched and Isoprenoid Tetraether (BIT) index was calculated from the concentrations of Branched GDGTs (tetramethyl-, pentamethyl-, and hexamethyl-GDGTs) and crenarchaeol using the following expression (Hopmans et al., 2004):

$$\text{BIT} = [\text{Branched GDGTs}]/([\text{Branched GDGTs}] + [\text{crenarchaeol}]).$$

4 Results

4.1 Branched and isoprenoid tetraether (BIT) index

The BIT index, a proxy for soil versus marine organic matter input to sediments (Hopmans et al., 2004), varied between 0.02 and 0.54, with an average of 0.14 (Fig. 4). The BIT index was higher in marine isotope stage (MIS) 6, MIS 4, and MIS 2 than in MIS 5, MIS 3, and MIS 1. The variation is consistent with the variation of δ^{18}O of benthic foraminifera (Fig. 4), suggesting that the mouth of the Mekong River came closer to the study site due to marine regression, resulting in an increase in soil organic matter input in the periods of low sea level stand.

4.2 TEX$_{86}^H$

Weijers et al. (2006) noted that samples with high BIT (> 0.4) may cause anomalously high TEX$_{86}^H$-derived temperatures. This was not a concern for most of the samples used in the present study. The samples showing BIT values higher than 0.4 were omitted for paleotemperature calculations in the profile in Fig. 4.

Applying a global core-top calibration (Kim et al., 2010), the TEX$_{86}^H$-derived temperature varied between 22.7 and 29.4 °C, with an average of 26.1 °C (Fig. 4). The TEX$_{86}^H$-derived temperature was ∼26 °C in MIS 6, ∼29.5 °C in MIS 5e, ∼26–28 °C in MIS 5d to 5a, ∼25 °C in MIS 4 to 2, and 28–29 °C in MIS 1 (Fig. 4). The core-top temperature was 28.1 °C, which agrees with the mean annual SST (27.9 °C; Conkright et al., 2002).

Recently, Jia et al. (2012) correlated core-top TEX$_{86}^H$ and water column temperature at 40 different sites in the SCS and found that the SSTs in the SCS were overestimated by a global core-top calibration (Kim et al., 2010). A correlation analysis indicated that TEX$_{86}^H$ correlated better with the mean annual temperature at 30–125 m ($r = 0.89$) than with the temperature in the 0–30 m mixed layer ($r = 0.69$). This suggests that TEX$_{86}^H$ reflects a deeper and cooler subsurface temperature, rather than the surface or mixed layer temperature in the SCS. Applying the SCS local core-top calibration (Jia et al., 2012), the TEX$_{86}^H$-derived temperature at 30–125 m varied between 18.0 and 23.4 °C, with an average of 20.7 °C (Fig. 4). The TEX$_{86}^H$-derived temperature was ∼20.5 °C in MIS 6, ∼23 °C in MIS 5e, ∼18–22 °C in MIS 5d to 5a, ∼20 °C in MIS 4 to 2, and 22–23 °C in MIS 1 (Fig. 4). The core-top temperature was 22.3 °C, which agrees with the mean annual temperature at ∼90 m (Conkright et al., 2002).

The TEX$_{86}^H$-derived temperature showed a suborbital-scale variation with an amplitude of > 1 °C (Fig. 4). Remarkable cooling occurred at 135 ka in MIS 6, 81 ka in MIS 5d, and 13 ka in the last deglaciation.

Title Page

Abstract | Introduction

Conclusions | References

Tables | Figures

|◄ | ►|

◄ | ►

Back | Close

Full Screen / Esc

Printer-friendly Version

Interactive Discussion

4.3 $U^{K'}_{37}$

The $U^{K'}_{37}$ in this core was reported by Zhao et al. (2006) and was also analyzed at lower resolution in the present study (Fig. 4). Column chromatography was used to separate alkenones in this study, but not in Zhao et al. (2006). Despite the difference in
5 preparation steps, both records showed an almost identical pattern (Fig. 4). One major difference was that the large cold excursion during 140–135 ka in the high-resolution record was not revealed in the new lower-resolution record. Applying a South China Sea core-top calibration (Pelejero and Grimalt, 1997), the $U^{K'}_{37}$-derived temperature obtained by Zhao et al. (2006) varied between 23.5 and 28.9 °C with an average of 26.2 °C
10 (Fig. 4). The $U^{K'}_{37}$-derived temperature was ∼ 26 °C in MIS 6, ∼ 29 °C in MIS 5e, ∼ 26–28 °C in MIS 5d to 5a, ∼ 25–26 °C in MIS 4 to 2, and 27–28 °C in MIS 1 (Fig. 4).

5 Discussion

5.1 Season and depth reflected by TEX^H_{86} and $U^{K'}_{37}$

In the western North Pacific (39° N, 147° E), the TEX_{86} in sinking particles did not
15 change seasonally and corresponded to the mean annual SST, suggesting that the GDGTs were produced by Thaumarchaeota throughout the entire year and homogenized in the surface and near surface water before sinking (Yamamoto et al., 2012). As indicated from satellite and shipboard observations, the chlorophyll concentrations did not display large seasonal variations, with only a moderate maximum in the winter
20 season in the study area (Feldman et al., 1989; Liu et al., 2002). These observations suggested that the production of GDGTs does not change seasonally, and that TEX^H_{86} reflected the mean annual temperature at the study site. Although the production depth of GDGTs and the depth at which TEX^H_{86} indicated temperature are still not clear, the investigation of surface sediments in the SCS suggested that TEX^H_{86} reflects a deeper

and cooler subsurface temperature, rather than the surface or mixed layer temperature, in the SCS (Jia et al., 2012). In the present study, we assumed that TEX_{86}^H reflected a subsurface mean annual temperature at 30–125 m.

The core-top $U_{37}^{K'}$-derived temperature obtained by the equations of Pelejero and Grimalt (1997) based on core-top calibration in the SCS and Prahl et al. (1988) based on calibration by a culture experiment were 27.9 and 27.0 °C, respectively. The former agrees with the mean annual SST (27.9 °C; Conkright et al., 2002), but the latter is 0.9 °C lower than the mean annual SST at the study site. The chlorophyll concentrations did not display large seasonal variations, with only a moderate maximum in the winter season in the study area (Feldman et al., 1989; Liu et al., 2002), suggesting that alkenone production continued throughout the entire year, but was more weighted in the winter season. The $U_{37}^{K'}$-derived temperature by Prahl's culture-based calibration thus indicates the SST weighted in winter, whereas that by the SCS core-top calibration indicates the mean annual SST. Because alkenone production is more weighted in winter, the variation of $U_{37}^{K'}$-derived temperature reflects more sensitively changes in winter SSTs.

Variation in the temperature at 30–125 m estimated using TEX_{86}^H ($T_{30-125m}$) was nearly parallel to the variation in the SST obtained from the study core using $U_{37}^{K'}$ (Zhao et al., 2006 and this study) (Fig. 4). The difference between the $U_{37}^{K'}$-derived SST and TEX_{86}^H-derived temperature at 30–125 m ($\Delta T_{alkenone-GDGT}$ as defined in Jia et al., 2012) varied between 3.2 and 8.7 °C with an average of 5.6 °C (Fig. 5). The $\Delta T_{alkenone-GDGT}$ was generally around 6 °C from 150 to 16 ka, dropped to 5 °C between 16 and 3 ka and rose to 6 °C after 3 ka (Fig. 5). Jia et al. (2012) suggested that $T_{alkenone-GDGT}$ is an index of the depth of the thermocline; higher $\Delta\Delta T_{alkenone-GDGT}$ indicates a shallow thermocline. If this is true, the lower $\Delta T_{alkenone-GDGT}$ in 16–3 ka reflected the thermocline deepening in this period. Although there were some changes, $\Delta T_{alkenone-GDGT}$ was nearly constant, suggesting that the thermocline structure of the SCS was stable in most periods during the last 150 kyr.

Full Screen / Esc

Printer-friendly Version

Interactive Discussion

In the present study, assuming that the depth profile of the water temperature was constant, the TEX_{86}^{H}-derived SST in the MD97-2151 core (SST^*) was obtained according to the following equation by adding the average value of $\Delta T_{\text{alkenone-GDGT}}$ (5.6 °C) during the last 150 kyr to the $T_{30-125m}$ (Fig. 6a):

$$SST^* [°C] = T_{30-125m} [°C] + 5.6.$$

5.2 Response of SCS SSTs to orbital forcing

Both TEX_{86}^{H}- and $U_{37}^{K'}$-derived temperatures (Fig. 4) showed a pattern that was broadly similar to that of $\delta^{18}O$ of benthic foraminifera (Fig. 4; Zhao et al., 2006) and the atmospheric CO_2 concentration recorded in Antarctic ice cores (Fig. 6b; Kawamura et al., 2007). The pattern was also similar to those of Mg/Ca-derived temperatures in the central WPWP region (Fig. 6b; ODP Site 806 in the Ontong Java Plateau; Lea et al., 2000 and MD97-2140 at the northern margin of New Guinea Island; de Garidel-Thoron et al., 2005). These correspondences suggest that the surface and subsurface temperatures in the southern SCS, together with the other regions of the WPWP regions and changes in atmospheric CO_2 concentration, responded principally to orbital forcing.

Detailed inspection, however, revealed that the SST change at the study site was delayed behind that in the central WPWP region and the changes in atmospheric CO_2 concentration (Fig. 6b). The delay in the response was evident in the periods from MIS 5d to MIS 3. Periodic cooling events occurred every 23 kyr and were superimposed on the variation seen in the other regions of the WPWP. To characterize the SST variations specific to the SCS, the SST at the study site was subtracted from the SSTs at ODP Site 806 (0°19′ N, 159°22′ E, 2520 m, Lea et al., 2000) and MD97-2140 (2°02′ N, 141°46′ E, 2547 m, de Garidel-Thoron et al., 2005). The SST record at MD97-2140 (de Garidel-Thoron et al., 2005) was reassessed in the present study by tuning the oxygen isotope profile of *G. ruber* to that of Martinson et al. (1987) (Fig. 6a). The SST difference ($SST_{WPWP} - SST_{SCS}$) was defined as ΔSST. Four different $\Delta SSTs$ (TEX_{86}^{H}-derived $\Delta SST^*_{ODP806-MD972151}$,

Full Screen / Esc

TEX$_{86}^{H}$-derived $\Delta SST^{*}_{MD972140\text{-}MD972151}$, U$_{37}^{K'}$-derived $\Delta SST_{ODP806\text{-}MD972151}$, U$_{37}^{K'}$-derived $\Delta SST_{MD972140\text{-}MD972151}$) showed a similar variation (Fig. 6c) and formed as a stacked ΔSST record (Fig. 6d). The stacked ΔSST showed a regular pattern, with cooler events every 23 kyr (Fig. 6d) and the best correlation with the May insolation at the equator.

5   The SCS is part of the Indo-Pacific Warm Pool region, but the winter surface temperature is significantly lower than that in the other regions of the WPWP. A recent oceanographic study demonstrated that this winter cooling is caused by the winter monsoon (Liu et al., 2004). Winter monsoon northerly winds cool the surface water in the northern margin of the SCS and advect the cooled water southward (Liu et al.,

10 2004). The SST in the study region is governed by the winter wind strength (Huang et al., 2011). These modern observations suggest that ΔSST is an index of the Asian winter monsoon activity with a lower ΔSST corresponding to a stronger winter monsoon. According to this interpretation, the East Asian winter monsoon varied in response to precessional forcing and was maximized at the May perihelion.

15   This variation is consistent with previously published shorter records of the East Asian winter monsoon based on SCS SSTs (Shintani et al., 2008; Huang et al., 2011) that showed an intensification of the East Asian winter monsoon during the last deglaciation and its gradual weakening during the Holocene. The variation is also consistent with a diatom record from the Huguang Maar Lake in south China that showed

20 an intensification of the East Asian winter monsoon during the last deglaciation and the early Holocene (Wang et al., 2012). Our result indicates that intensification of the Asian winter monsoon also occurred in the penultimate deglaciation (glacial termination II), and the variation has responded to a precessional cycle.

    Cross-spectral analysis between ΔSST and the $\delta^{18}O$ of benthic foraminifera in a

25 period of 7 to 145 ka indicates that the periodicity at 23 kyr is dominant and highly coherent at this frequency (Fig. 7). The ΔSST maximum lags the precession maximum (the Northern Hemisphere summer insolation minimum) by $138° \pm 19°$ (8.8 ± 1.2 kyr) in the precession band (Fig. 8). The ΔSST best fits the insolation of mid-May at the equator (Fig. 6d).

Title Page

Abstract   Introduction

Conclusions   References

Tables   Figures

|◄   ►|

◄   ►

Back   Close

Full Screen / Esc

Printer-friendly Version

Interactive Discussion

On a 23-kyr cycle, the maximum phase of the winter monsoon (maximum ΔSST) corresponds to the May perihelion (Fig. 8). However, this perspective is not consistent with the hypotheses proposed by previous studies. The Kutsubach model hypothesized that the winter monsoon was maximum at the June perihelion. Huang et al. (1997a), Wang et al. (1999), and de Garidel-Thoron et al. (2001) suggested that the winter monsoon was maximal when the continental ice volume was maximal (around the March perihelion). In contrast to these studies, our work suggests that the winter monsoon was maximal at the May perihelion.

The results of the present study also showed that the variation in the East Asian winter monsoon was nearly anti-phase with the variation in the Indian summer monsoon. The phase of the Indian summer monsoon stack was reconstructed using marine upwelling records from the Arabian Sea, and the maximum phase of the summer monsoon corresponded to the October to November perihelion (Fig. 8; Clemens and Prell, 2003; Caley et al., 2011). The phase of the Indian summer monsoon was thus anti-phase with the East Asian winter monsoon suggested by ΔSST in the present study. Caley et al. (2011) assigned upwelling and non-upwelling assemblages of planktonic foraminifera to the summer and winter monsoon assemblages, respectively, in a core from the Arabian Sea. Based on the record of these assemblages, they suggested that the Indian winter monsoon was anti-phase with the summer monsoon stack and maximal at the May perihelion. Because the relative abundance of the winter monsoon assemblage was affected mainly by the abundance of the summer monsoon assemblage (Caley et al., 2011), the phase of the winter monsoon assemblage maxima must be considered with caution. Despite this, the phase coincided with the maximum phase of the East Asian winter monsoon proposed in this study. This correspondence supports the perspective of Caley et al. (2011) that the Indian summer and winter monsoons were in anti-phase in the precession band. It also suggests that the Asian winter monsoon system behaved synchronously in the East Asian and Indian regions.

On a 23-kyr cycle, the variation in ΔSST was out-of-phase by $\sim 80°$ with changes in the East Asian summer monsoon intensity suggested by the stalagmite oxygen iso-

tope record from the Hulu and Sanbao caves in central China (Fig. 8; Wang et al., 2001, 2008). However it was anti-phase with changes in the summer monsoon precipitation in central Japan, as demonstrated by a pollen record from MD01-2421 (Fig. 8; Igarashi and Oba, 2006). The mismatch in the phase of variation between stalagmite

5 and pollen records suggests that the response of precipitation to changes in the East Asian summer monsoon was regionally variable (Yamamoto, 2009) or that the oxygen isotopes of Chinese stalagmites were not a simple proxy of summer precipitation, but were also affected by winter temperatures in China (Clemens et al., 2010). The summer precipitation in central Japan was stronger when the East Asian winter monsoon

10 was weaker, and vice versa. This correspondence suggests that the East Asian winter monsoon was linked to an aspect of the East Asian summer monsoon that was related to precipitation in Japan, i.e. the position of the early rain front (Baiu Front) and/or the intensity of its activity.

The Asian monsoon system transfers energy and water vapor across the equator.

15 The ΔSST record suggests that the East Asian winter monsoon was weakest when perihelion occurred in November. At the same phase, the Indian summer monsoon was strongest and transferred more heat from the Southern Hemisphere to the Northern Hemisphere, resulting in warming in the Northern Hemisphere and cooling in the Southern Hemisphere. In contrast, when perihelion occurred in May, the East Asian

20 winter monsoon was strongest and the Indian summer monsoon was weakest. The monsoon system transferred more energy to the Southern Hemisphere, resulting in cooling in the Northern Hemisphere and warming in the Southern Hemisphere. According to this perspective, the Asian monsoon system was involved in the regulation of heat balance over both hemispheres on an orbital timescale.

25 Two possible interpretations are proposed for the fact that the East Asian winter monsoon was maximum at the May perihelion rather than at the ice volume maxima (the March perihelion) or the insolation minimum at boreal winter (the June perihelion). First, the May perihelion is an intermediate between the ice volume maximum and the insolation minimum in boreal winter. The combined effect of cooling by ice volume forc-

ing and the decrease in winter insolation could result in a maximum in the East Asian winter monsoon at the May perihelion. Second, the weakest Indian summer monsoon decreased the heat transfer from the Southern Hemisphere to the Northern Hemisphere and cooled Siberia in winter, causing a stronger Siberian High then. In both cases, the East Asian winter monsoon was driven by inter-hemispheric heat balance. The variation was linked to variations in the Indian summer and winter monsoons, and thus is regarded as a part of the process driving climate change in the regions from the southern Indian Ocean, Australia, South to East Asia, and the North Pacific.

6 Conclusions

The sea surface temperature difference (ΔSST) between the South China Sea and other Western Pacific Warm Pool regions reflected the intensity of the Asian winter monsoon. The ΔSST showed significant precession cycles during the last 150 kyr. In the precession cycle, the maximum winter monsoon intensity shown by the ΔSST was delayed behind the maximum ice volume, and the East Asian winter monsoon was anti-phase with the Indian summer monsoon and the summer monsoon precipitation in central Japan. Our results suggest that the phase of the East Asian winter monsoon reflects a physical mechanism of inter-hemispheric heat balance.

References

Caley, T., Malaizé, B., Zaragosi, S., Rossignol, L., Bourget, J., Eynaud, F., Martinez, P., Giraudeau, J., Charlier, K., and Ellouz-Zimmermann, N.: New Arabian Sea records help decipher orbital timing of Indo-Asian monsoon, Earth Planet. Sc. Lett., 308, 433–444, 2011.

Chen, M.-T. and Huang, C.-Y.: Ice-volume forcing of winter monsoon climate in the South China Sea, Paleoceanography, 13, 622–633, 1998.

Chen, M.-T., Beaufort, L., and the Shipboard Scientific Party of the IMAGES III/MD106-IPHIS Cruise (Leg II): Exploring Quaternary variability of the East Asian monsoon, Kuroshio Current, and the Western Pacific warm pool systems: high-resolution investigations of paleoceanography from the IMAGES III/MD106-IPHIS cruise, Terr. Atmos. Ocean. Sci., 9, 129–142, 1998.

Chen, M.-T., Shiau, L.-J., Yu, P.-S., Chiu, T.-C., Chen, Y.-G., and Wei, K.-Y.: 500 000-Year records of carbonate, organic carbon, and foraminiferal sea surface temperature from the southeastern South China Sea (near Palawan Island), Palaeogeogr. Palaeocl., 197, 113–131, 2003.

Clemens, S. C. and Prell, W. L.: A 350,000 year summer-monsoon multi-proxy stack from the Own Ridge, Northern Arabian Sea, Mar. Geol., 201, 35–51, 2003.

Conkright, M. E., Locarnini, R. A., Garcia, H. E., O'Brien, T. D., Boyer, T. P., Stephens, C., and Antonov, J. I.: World Ocean Atlas 2001: Objective Analyses, Data Statistics, and Figures, CD-ROM Documentation. National Oceanographic Data Center, Silver Spring, MD, 17 pp., 2002.

de Garidel-Thoron, T., Beaufort, L., Linsley, B. K., and Dannenmann, S.: Millennial-scale dynamics of the East Asian winter monsoon during the last 200,000 years, Paleoceanography, 16, 491–502, 2001.

de Garidel-Thoron, T., Rosenthal, Y., Bassinot, F., and Beaufort, L.: Stable sea surface temperatures in the western Pacific warm pool over the past 1.75 million years, Nature, 433, 294–298, 2005.

Ding, Z., Liu, T., Putter, N. W., Yu, Z., Guo, Z., and Zhu, R.: Ice-volume forcing of East Asian winter monsoon variations in the past 800,000 years, Quaternary Res., 44, 149–159, 1995.

Feldman, G. C., Kuring, N., Ng, C., Esaias, W., McClain, C., Elrod, J., Maynard, N., and Endres, D.: Ocean color-availability of the global data set, Eos Transactions American Geophysical Union, 70, 634, 1989.

The East Asian winter monsoon variability

M. Yamamoto et al.

Title Page

Abstract | Introduction

Conclusions | References

Tables | Figures

◄ | ►

◄ | ►

Back | Close

Full Screen / Esc

Printer-friendly Version

Interactive Discussion

Hopmans, E. C., Schouten, S., Pancost, R., van der Meer, M. T. J., and Sinninghe Damsté, J. S.: Analysis of intact tetraether lipids in archaeal cell material and sediments by high performance liquid chromatography/atmospheric pressure chemical ionization mass spectrometry, Rapid Commun. Mass Spectrom., 14, 585–589, 2000.

Hopmans, E. C., Weijers, J. W. H., Schefuß, E., Herfort, L., Sinninghe Damsté, J. S., and Schouten, S.: A novel proxy for terrestrial organic matter in sediments normalized on branched and isoprenoid tetraether lipids, Earth Planet. Sc. Lett., 224, 107–116, 2004.

Huang, C.-C., Chen, M.-T., Lee, M.-Y., Wei, K.-Y., and Huang, C.-Y.: Planktic foraminifer faunal sea surface temperature records of the past two glacial terminations in the South China Sea near Wan-An shallow (IMAGES core MD972151), West. Pacific Earth Sci., 2, 1–14, 2002.

Huang, C.-Y., Liew, P.-M., Zhao, M., Chang, T.-C., Kuo, C.-M., Chen, M.-T., Wang, C.-H., and Zheng, L.: Deep sea and lake records of the Southeast Asian paleomonsoons for the last 25 kyrs, Earth Planet. Sc. Lett., 146, 59–72, 1997a.

Huang, C.-Y., Wu, S.-F., Zhao, M., Chen, M.-T., Wang, C.-H., Tu, X., and Yuan, P. B.: Surface ocean and monsoon climate variability in the South China Sea since last glaciation, Mar. Micropaleontol., 32, 71–94, 1997b.

Huang, C. Y., Wang, C. C., and Zhao, M.: High-resolution carbonate stratigraphy of IMAGES core MD972151 from the South China Sea, Terr. Atmos. Ocean. Sci., 10, 225–238, 1999.

Huang, E., Tian, J., and Steinke, S.: Millennial-scale dynamics of the winter cold tongue in the southern South China Sea over the past 26 ka and the East Asian winter monsoon, Quaternary Res., 75, 196–204, 2011.

Igarashi, Y. and Oba, T.: Fluctuations of monsoons and insolation in the northwest Pacific during the last 144 kyr from a high-resolution pollen analysis of the IMAGES core MD01-2421, Quaternary Sci. Rev., 25, 1447–1459, 2006.

Jia, G., Zhang, J., Chen, J., Peng, P., and Zhang, C. L.: Archaeal tetraether lipids record subsurface water temperature in the South China Sea, Org. Geochem., 50, 68–77, 2012.

Kawamura, K., Parrenin, F., Lisiecki, L., Uemura, R., Vimeux, F., Severinghaus, J. P., Hutterli, M. A., Nakazawa, T., Aoki, S., Jouzel, J., Raymo, M. E., Matsumoto, K., Nakata, H., Motoyama, H., Fujita, S., Goto-Azuma, K., Fujii, Y., and Watanabe, O.: Northern Hemisphere forcing of climatic cycles in Antarctica over the past 360,000 years, Nature, 448, 912–917, 2007.

Kienast, M., Steinke, S., Stattegger, K., and Calvert, S. E.: Synchronous tropical South China Sea SST changes and Greenland warming during deglaciation, Science, 291, 2132–2134, 2001.

The East Asian winter monsoon variability

M. Yamamoto et al.

Title Page

Abstract | Introduction

Conclusions | References

Tables | Figures

|◄ | ►|

◄ | ►

Back | Close

Full Screen / Esc

Printer-friendly Version

Interactive Discussion

Kim, J.-H., van der Meer, J., Schouten, S., Helmke, P., Willmott, V., Sangiorgi, F., Koc, N., Hopmans, E. C., and Sinninghe Damsté, J. S.: New indices and calibrations derived from the distribution of crenarchaeal isoprenoid tetraether lipids: Implications for past sea surface temperature reconstructions, Geochim. Cosmochim. Acta, 74, 4639–4654, 2010.

Kutzbach, J.: Monsoon climate of the Early Holocene: Climate experiment with the Earth's orbital parameters for 9000 years ago, Science, 214, 59–61, 1981.

Lea, D. W., Pak, D. K., and Spero, H. J.: Climate impact of Late Quaternary equatorial Pacific sea surface temperature variations, Science, 289, 1719–1724, 2000.

Lee, M.-Y., Wei, K.-Y., and Chen, Y.-G.: High resolution oxygen isotope stratigraphy for the lat 150,000 years in the southern South China Sea: Core MD972151, Terr. Atmos. Ocean. Sci., 10, 239–254, 1999.

Lee, T.-Q.: Last 160 ka paleomagnetic directional secular variation record from core MD972151, southern South China Sea, Terr. Atmos. Ocean. Sci., 10, 255–264, 1999.

Li, D., Zhao, M., Tian, J., and Li, L.: Comparison and implication of TEX_{86} and $U^{K'}_{37}$ temperature records over the last 356 kyr of ODP Site 1147 from the northern South China Sea, Palaeogeogr. Palaeocl., 376, 213–223, 2013.

Liu, K.-K., Chao, S.-Y., Shaw, P.-T., Gong, C.-C., Chen, C.-C., and Tang, T. Y.: Monsoon-forced chlorophyll distribution and primary production in the South China Sea: observations and a numerical study, Dee-Sea Res. Pt. I, 46, 1387–1412, 2002.

Liu, Q., Jiang, X., Xie, S. P., and Liu, W. T.: A gap in the Indo-Pacific warm pool over the South China Sea in boreal winter: Seasonal development and interannual variability, J. Geophys. Res., 109, C07012, doi:10.1029/2003JC002179, 2004.

Martinson, D. G., Pisias, N. G., Hays, J. D., Imbrie, J., Moore Jr., T. C., and Shackleton, N. J.: Age dating and the orbital theory of the ice ages: Development of a high-resolution 0 to 300,000-year chronostratigraphy, Quaternary Res., 27, 1–29, 1987.

NOAA: http://iridl.ldeo.columbia.edu/SOURCES/.NOAA/.NODC/.WOA98/ (last access: 5 July 2013), 1998.

Oppo, D. W. and Sun, Y.: Amplitude and timing of sea-surface temperature changes in the northern South China Sea: Dynamic link to the East Asian monsoon, Geology, 33, 785–788, 2005.

Paillard, D., Labeyrie, L., and Yion, P.: Macintosh program performs time-series analysis, EOS Trans. AGU, 77, 379, 1996.

Pelejero, C. and Grimalt, J. O.: The correlation between $U_{37}^{K'}$ index and sea surface temperatures in the warm boundary: The South China Sea, Geochim. Cosmochim. Acta, 61, 4789–4797, 1997.

Pelejero, C., Grimalt, J. O., Heilig, S., Kienast, M., and Wang, L.: High-resolution $U_{37}^{K'}$ temperature reconstructions in the South China Sea over the past 220 kyr, Paleoceanography, 14, 224–231, 1999.

Prahl, F. G., Muehlhausen, L. A., and Zahnle, D. L.: Further evaluation of long-chain alkenones as indicators of paleoceanographic conditions, Geochim. Cosmochim. Acta, 52, 2303–2310, 1988.

Reimer, P. J., Baillie, M. G. L., Bard, E., Bayliss, A., Beck, J. W., Bertrand, C. J. H., Blackwell, P. G., Buck, C. E., Burr, G. S., Cutler, K. B., Damon, P. E., Edwards, R. L., Fairbanks, R. G., Friedrich, M., Guilderson, T. P., Hogg, A. G., Hughen, K. A., Kromer, B., McCormac, F. G., Manning, S. W., Ramsey, C. B., Reimer, R. W., Remmele, S., Southon, J. R., Stuiver, M., Talamo, S., Taylor, F. W., van der Plicht, J., and Weyhenmeyer, C. E.: IntCal04 Terrestrial radiocarbon age calibration, 26–0 ka BP, Radiocarbon, 46, 1029–1058, 2004.

Schouten, S., Hopmans, E. C., Schefuß, E., and Sinninghe Damsté, J. S.: Distributional variations in marine crenarchaeotal membrane lipids: a new tool for reconstructing ancient sea water temperatures?, Earth Planet. Sc. Lett., 204, 265–274, 2002.

Schouten, S., Huguet, C., Hopmans, E. C., Kienhuis, M. V. M., and Sinninghe Damsté, J. S.: Analytical methodology for TEX$_{86}$ paleothermometry by high performance liquid chromatography/atmospheric pressure chemical ionization-mass spectrometry, Anal. Chem., 79, 2940–2944, 2007.

Shintani, T., Yamamoto, M., and Chen, M.-T.: Slow warming of the northern South China Sea during the last deglaciation, Terr. Atmos. Ocean. Sci., 19, 341–346, 2008.

Shintani, T., Yamamoto, M., and Chen, M.-T.: Paleoenvironmental changes in the northern South China Sea over the past 28,000 years: a study of TEX$_{86}$-derived sea surface temperatures and terrestrial biomarkers, J. Asian Earth Sci., 40, 1221–1229, 2011.

Steinke, S., Kienast, M., Groeneveld, J., Lin, J.-C., Chen, M.-T., and Rendle-Bühring, R.: Proxy dependence of the temporal pattern of deglacial warming in the tropical South China Sea: toward resolving seasonality, Quaternary Sci. Rev., 27, 688–700, 2008.

Tian, J., Huang, E., and Park, D. K.: East Asian monsoon variability over the last glacial cycle: Insights from a latitudinal sea-surface temperature gradient across the South China Sea, Palaeogeogr. Palaeocl., 292, 319–324, 2010.

Title Page

Abstract | Introduction

Conclusions | References

Tables | Figures

|◀ | ▶|

◀ | ▶

Back | Close

Full Screen / Esc

Printer-friendly Version

Interactive Discussion

Wang, B., Clemens, S. C., and Liu, P.: Contrasting the Indian and East Asian monsoons: implications on geologic timescales, Mar. Geol., 201, 5–21, 2003.

Wang, L. and Wang, P.: Late Quaternary paleoceanography of the South China Sea: Glacial–interglacial contrasts in an enclosed basin, Paleoceanography, 5, 77–90, 1990.

Wang, L., Sarnthein, M., Erlenkeuser, H., Grimalt, J. O., Grootes, P. M., Heilig, S., Ivanova, E., Kienast, M., Pelejero, C., and Pflaumann, U.: East Asia monsoon climate during the late Pleistocene: high-resolution sediment records from the South China Sea, Mar. Geol., 156, 245–284, 1999.

Wang, L., Li, J., Lu, H., Gu, Z., Rioual, P., Hao, Q., Mackay, A. W., Jiang, W., Cai, B., Xu, B., Han, J., and Chu, G.: The East Asian winter monsoon over the last 15,000 years: its links to high-latitudes and tropical climate systems and complex correlation to the summer monsoon, Quaternary Sci. Rev., 32, 131–142, 2012.

Wang, P., Wang, L., Bian, Y., and Jian, Z.: Late Quaternary paleoceanography of the South China Sea: surface circulation and carbonate cycles, Mar. Geol., 127, 145–165, 1995.

Wang, Y. J., Cheng, H., Edwards, R. L., An, Z. S., Wu, J. Y., Shen, C.-C., and Dorale, J. A.: A High-Resolution Absolute-Dated Late Pleistocene Monsoon Record from Hulu Cave, China, Science, 294, 2345–2348, 2001.

Wang, Y. J., Cheng, H., Edwards, R. L., Kong, X., Shao, X., Chen, S., Wu, J., Jiang, X., Wang, X., and An, Z.: Millennial- and orbital-scale changes in the East Asian monsoon over the past 224,000 years, Nature, 451, 1090–1093, 2008.

Weijers, J. W. H., Schouten, S., Spaargaren, O. C., and Sinninghe Damsté, J. S.: Occurrence and distribution of tetraether membrane in soils: Implications for the use of the BIT index and the TEX$_{86}$ SST proxy, Org. Geochem., 37, 1680–1693, 2006.

Wuchter, C., Schouten, S., Coolen, M. J. L., and Sinninghe Damsté, J. S.: Temperature-dependent variation in the distribution of tetraether membrane lipids of marine Crenarchaeota: Implications for TEX$_{86}$ paleothermometry, Paleoceanography, 19, PA4028, doi:10.1029/2004PA001041, 2004.

Wyrtki, K.: Physical oceanography of the southeast Asia waters, in: Scientific Results of Maritime Investigations of the South China Sea and the Gulf of Thailand 1959–1961, Naga Rep. 2, Scripps Institute of Oceanography, La Jolla, California, USA, 1961.

Xiao, J., Porter, S. C., An, Z., Kumai, H., and Yoshikawa, S.: Grain size of quartz as an indicator of winter monsoon strength on the loess plateau of central China during the last 130,000 yr, Quaternary Res., 43, 22–29, 1995.

The East Asian winter monsoon variability

M. Yamamoto et al.

Yamamoto, M.: Response of mid-latitude North Pacific surface temperatures to orbital forcing and linkage to the East Asian summer monsoon and tropical ocean-atmosphere interactions, J. Quaternary Sci., 24, 836–847, 2009.

Yamamoto, M. and Polyak, L.: Changes in terrestrial organic matter input to the Mendeleev Ridge, western Arctic Ocean, during the Late Quaternary, Global Planet. Change, 68, 30–37, 2009.

Yamamoto, M., Shimamoto, A., Fukuhara, T., Tanaka, Y., and Ishizaka, J.: Glycerol dialkyl glycerol tetraethers and the TEX_{86} index in sinking particles in the western North Pacific, Org. Geochem., 53, 52–62, 2012.

Yuan, D., Cheng, H., Lawrence, E. R., Dykoski, C. A., Kelly, M. J., Zhang, M., Qing, J., Lin, Y., Wang, Y., Wu, J., Dorale, J. A., An, Z., and Cai, Y.: Timing, Duration, and Transitions of the Last Interglacial Asian Monsoon, Science, 304, 575–578, 2004.

Zhang, J., Bai, Y., Xu, S., Lei, X., and Jia, G.: Alkenone and tetraether lipids reflect different seasonal seawater temperatures in the coastal northern South China Sea, Org. Geochem., 58, 115–120, 2013.

Zhao, M., Huang, C.-Y., Wang, C.-C., and Wei, G.: A millennial-scale sea surface temperature record from the South China Sea (8° N) over the last 150 kyr: Monsoon and sea-level influence, Palaeogeogr. Palaeocl., 236, 39–55, 2006.

Zielinski, G. A., Mayewski, P. A., Meeker, L. D., Whitlow, S., and Twicker, M. S.: Potential atmospheric impact of the Toba megaeruption ~ 71,000 years ago, Geophys. Res. Lett., 23, 837–840, 1996.

Table 1. Control points for the age model for core MD97-2151.

Depth (cm)	Conventional age (yr)	Calendar age (yr BP)	Source (foraminifera species)	Reference
3	1437 ± 66	938	^{14}C (*G. sacculifer*)	Zhao et al. (2006)
35	1897 ± 56	1353	^{14}C (*G. sacculifer*)	Zhao et al. (2006)
71	2575 ± 56	2143	^{14}C (*G. sacculifer*)	Zhao et al. (2006)
91	2986 ± 67	2743	^{14}C (*G. sacculifer*)	Zhao et al. (2006)
127	3869 ± 65	3697	^{14}C (*G. sacculifer*)	Zhao et al. (2006)
171	4404 ± 57	4499	^{14}C (*G. sacculifer*)	Zhao et al. (2006)
211	5323 ± 67	5648	^{14}C (*G. sacculifer*)	Zhao et al. (2006)
251	6810 ± 66	7276	^{14}C (*G. sacculifer*)	Zhao et al. (2006)
311	9329 ± 72	9927	^{14}C (*G. sacculifer*)	Zhao et al. (2006)
551.5	13 900 ± 90	16 034	^{14}C (*G. sacculifer*)	This study
599.5	15 540 ± 90	18 261	^{14}C (*G. sacculifer*)	This study
651.5	18 160 ± 105	20 957	^{14}C (*G. sacculifer*)	This study
699.5	17 680 ± 100	20 387	^{14}C (*G. sacculifer*)	This study, not used for age model
801.5	19 305 ± 105	22 418	^{14}C (*G. sacculifer*)	This study
1085.5		43 880	MIS 3.13	Zhao et al. (2006)
1313		58 960	MIS 4.0	Zhao et al. (2006)
1421		64 090	MIS 4.22	Zhao et al. (2006)
1556		71 000	Toba ash layer	Zhao et al. (2006)
1601		73 910	MIS 5.0	Zhao et al. (2006)
1653		79 250	MIS 5.1	This study
1785		96 210	MIS 5.31	This study
1845		103 290	MIS 5.33	This study
1949		110 790	MIS 5.4	Zhao et al. (2006)
2097		122 560	MIS 5.51	Zhao et al. (2006)
2133		125 190	MIS 5.53	Zhao et al. (2006)
2197		129 840	MIS 6.0	Zhao et al. (2006)
2321		135 100	MIS 6.2	Zhao et al. (2006)

Full Screen / Esc

Printer-friendly Version

Interactive Discussion
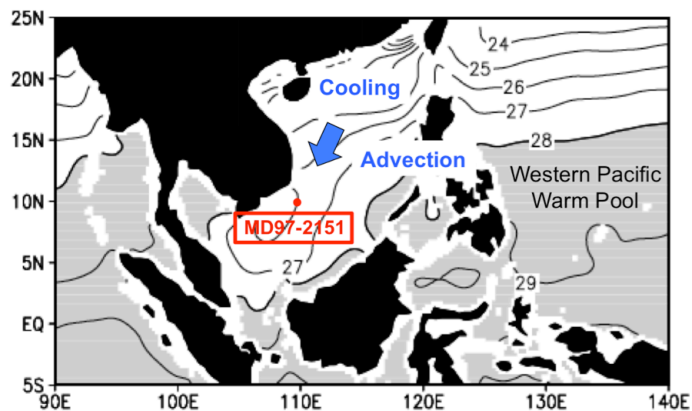
Fig. 1. Map showing the location of core MD97-2151 and the winter sea surface temperatures in the South China Sea (Liu et al., 2004).
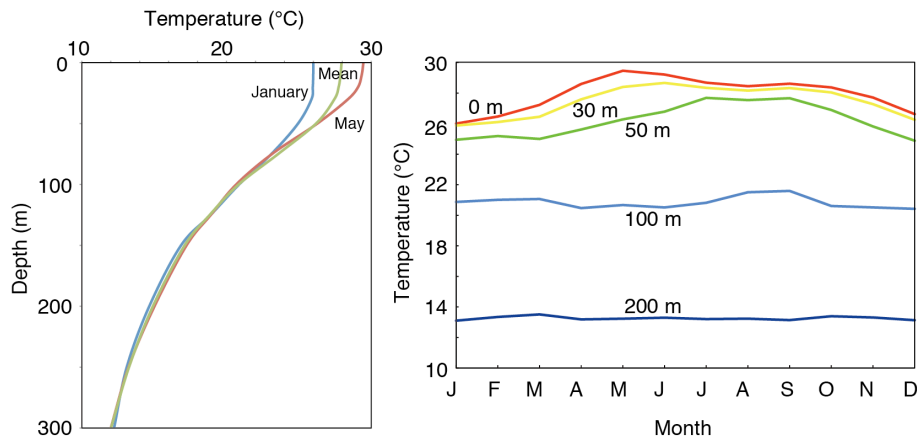
Fig. 2. Depth and seasonal variation of water temperatures at the study site (compiled data from NOAA, 1998). Months "J" to "D" means January to December.
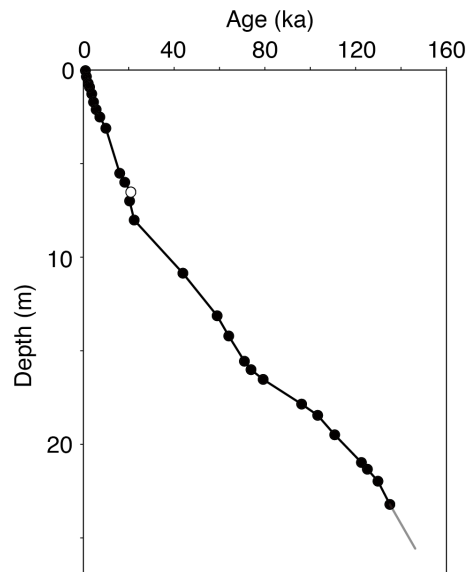
Fig. 3. Age depth model of core MD97-2151 (Zhao et al., 2006 and this study). The age at 699.5 m (open circle) was not used for the age-depth model.
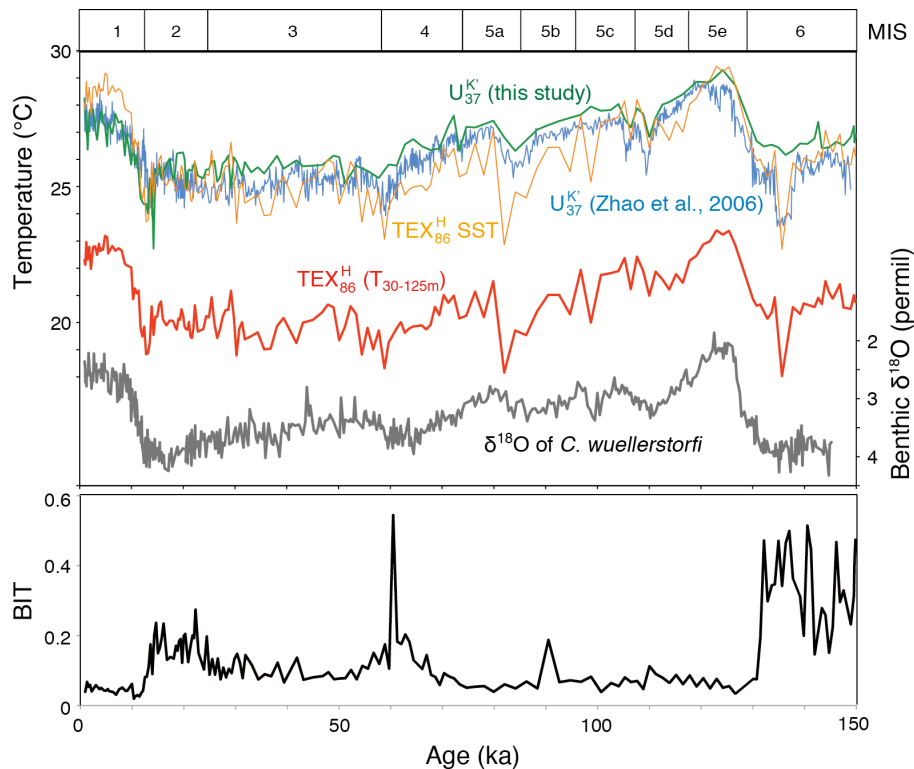
Fig. 4. TEX$_{86}^{H}$-derived SST (this study), TEX$_{86}^{H}$-derived temperature at 30–125 m ($T_{30-125m}$; this study), U$_{37}^{K'}$-derived SST (Zhao et al., 2006 and this study), δ^{18}O of *Cibicidoides wuellerstorfi* (Zhao et al., 2006), and the BIT index value (this study) in core MD97-2151.
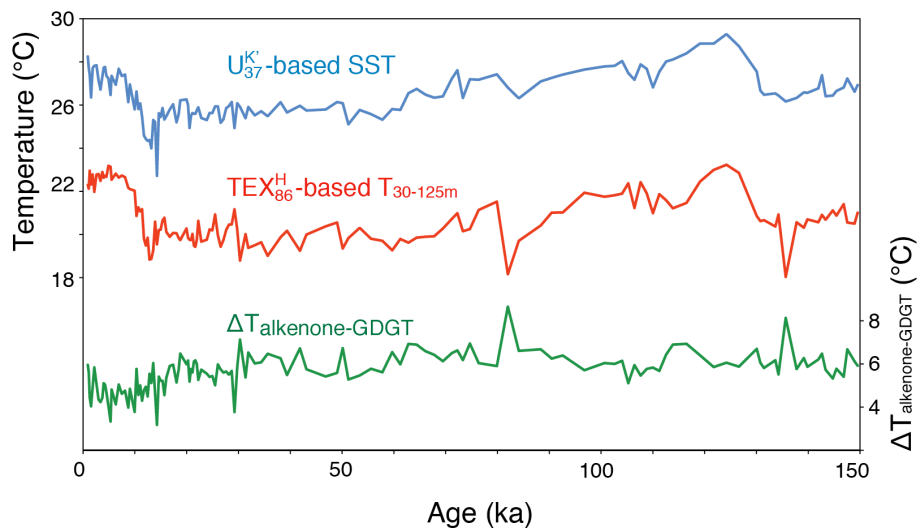
Fig. 5. TEX_{86}^{H}-derived temperatures at 30–125 m ($T_{30-125m}$), $U_{37}^{K'}$-derived SST (this study), and the difference between $U_{37}^{K'}$-derived SST and T at 30–125 m ($\Delta T_{alkenone-GDGT}$) in core MD97-2151.

Full Screen / Esc

Printer-friendly Version

Interactive Discussion

Fig. 6. (A) $\delta^{18}O$ of benthic foraminifera (BF) in core MD97-2151 (Zhao et al., 2006) and of planktonic foraminifera (PF) in ODP 806 (Lea et al., 2000) and core MD97-2140 (de Garidel-Thoron et al., 2005). **(B)** TEX_{86}^{H}-derived SSTs* and $U_{37}^{K'}$-derived SSTs in core MD97-2151 (red and orange lines, respectively), Mg/Ca-derived SSTs in core MD97-2140 (yellow line; de Garidel-Thoron et al., 2005), and ODP 806 (purple line; Lea et al., 2000), and CO_2 concentrations from Dome Fuji (Kawamura et al., 2007). **(C)** Temperature differences (ΔSSTs) between the central western Pacific warm pool region (MD97-2140 and ODP 806) and Site MD97-2151 in the southern South China Sea. **(D)** The stacked ΔSST. The insolation on 13 November at the equator is shown for comparison. Temperatures were calculated from $U_{37}^{K'}$ using an equation based on the core-top calibration (Pelejero and Grimalt, 1997). SST* [°C] = $T_{30-125m}$ [°C] + 5.6.
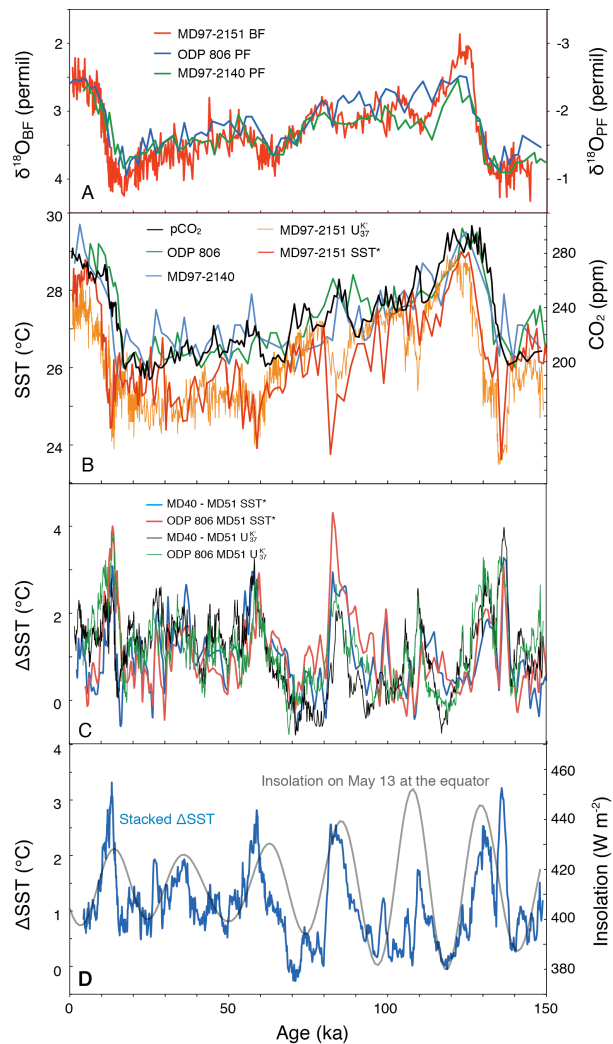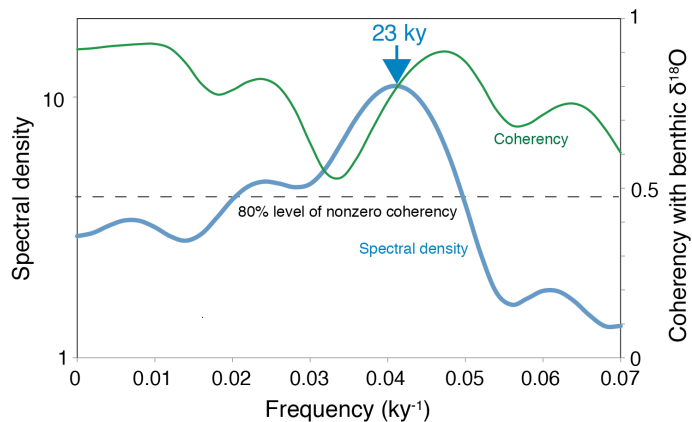
Fig. 7. Power spectrum of the variation in ΔSST during 4.3–145.1 ka. The bandwidth is 0.022. We performed spectral analyses using the Blackman–Tukey and Cross–Blackman–Tukey methods provided in the Analyseries software package (Paillard et al., 1996).
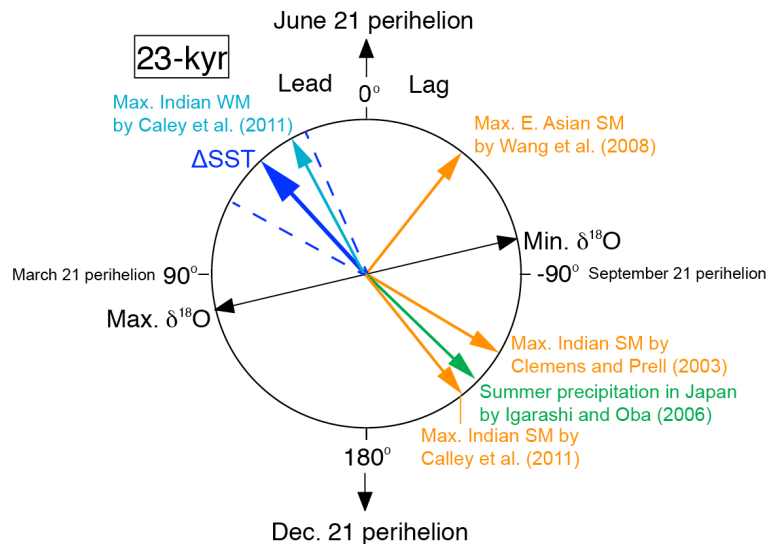
Fig. 8. Precession wheel showing the phases of stacked ΔSST maxima (with errors of the estimate shown by the dashed lines), the Indian summer monsoon stack maxima (Clemens and Prell, 2003), the Indian summer and winter monsoon maxima (Caley et al., 2011), the East Asian summer monsoon maxima (Wang et al., 2008), and the maxima of the summer precipitation in central Japan (Igarashi and Oba, 2006).